International Journal of Pharmaceutics 429 (2012) 113–122

Contents lists available at SciVerse ScienceDirect

International Journal of Pharmaceutics

journal homepage: www.elsevier.com/locate/ijpharm

Pharmaceutical Nanotechnology

Magnetic micelles as a potential platform for dual targeted drug delivery in cancer therapy

Chi Huang[a], Zhaomin Tang[a], Yangbo Zhou[b], Xiaofeng Zhou[c], Yong Jin[c], Dan Li[a], Ying Yang[a], Shaobing Zhou[a,b,*]

[a] School of Materials Science and Engineering, Key Laboratory of Advanced Technologies of Materials, Ministry of Education, Southwest Jiaotong University, Chengdu 610031, PR China
[b] School of Life Science and Engineering, Southwest Jiaotong University, Chengdu 610031, Sichuan, PR China
[c] Interventional Therapy Department, The Second Affiliated Hospital, Soochow University, 215004 Suzhou, PR China

ARTICLE INFO

Article history:
Received 12 November 2011
Received in revised form 3 March 2012
Accepted 4 March 2012
Available online 8 March 2012

Keywords:
Micelles
Targeted drug delivery
Magnetic nanoparticles
Cancer therapy

ABSTRACT

The magnetic nanomicelles as a potential platform for dual targeted (folate-mediated and magnetic-guided) drug delivery were developed to enhance the efficiency and veracity of drug delivering to tumor site. The magnetic nanocarriers were synthesized based on superparamagnetic iron oxide nanoparticles (SPIONs), biocompatible Pluronic F127 and poly(DL-lactic acid) (F127-PLA) copolymer chemically conjugated with tumor-targeting ligand-folic acid (FA) *via* a facile chemical conjugation method. Doxorubicin hydrochloride (DOX·HCl) was selected as a model anticancer drug to investigate the *in vitro* drug release and antiproliferative effect of tumor cells *in vitro* and *in vivo* in the presence or absence of an external magnetic filed (MF) with strength of 0.1 T. The Alamar blue assay exhibited that these magnetic nanomicelles possessed remarkable cell-specific targeting *in vitro*. Additionally this smart system enabling folate receptor-mediated uptake into tumor cells, showed strong responsiveness to MF. The primary *in vivo* tumor model study, which was carried out in VX2 tumor-bearing male New Zealand white rabbits, demonstrated that the nanomicelles could be guided into tumor site more efficiently by application of MF, and further represented significant therapeutic efficiency to solid tumor.

1. Introduction

Magnetic materials in nanoscale could provide exciting advantage for targeted drug delivery (Lee et al., 2009; Zhu et al., 2008; Gautier et al., 2011), magnetic resonance imaging (Fan et al., 2011; Ma et al., 2007), bioseparation (Zhuo et al., 2009; Wang et al., 2006), biosensor (Wang et al., 2010; Liu et al., 2008) and hyperthermia (Hou et al., 2009). Superparamagnetic iron oxide nanoparticles (SPIONs) as the typical magnetic nanoparticles are also becoming prominent. Although, bare SPIONs exert some toxic effects, coated SPIONs have been found to be relatively nontoxic (Lewinski et al., 2008), they were approved by the US Food and Drug Administration (FDA) due to the quite benign toward humans (Ke et al., 2010; Lee et al., 2007; Lattuada and Hatton, 2007). Additionally, they can be guided and maintained to the precise location with external magnetic field. Furthermore, magnetic actuation has been explored for 'distant' control and site targeted delivery. Thus, integration of SPIONs with biological molecules and therapeutics creates smart materials with advanced properties (Wu et al., 2010; Kim et al., 2010).

Cancer remains one of the world's most devastating diseases. However, currently anti-cancer drug, which suffer from limited efficacy and side effects, often kill healthy cells and cause toxicity to the patient (Peer et al., 2007). In recent years, the targeted drug delivery systems have been extensively studied in cancer treatments. It can deliver the drug to anticipated target site thereby reducing the drug toxicity and increasing the therapeutic efficacy (Peer et al., 2007; Munniera et al., 2008). SPIONs especially in targeted drug delivery have been investigated because of their novel abilities to target the specific locations, consequently minimizing severe side effects taken from anti-cancer drug (Yu et al., 2008). The drug loaded SPIONs can be guided and concentrated in anticipated targeting site by application of an external magnetic field, consequently, the therapeutic effects of drugs can be enhanced (Won et al., 2005; Allen and Cullis, 2004; Pradhan et al., 2010). Recently another strategy for enhancing the efficiency of drug delivery would be to conjugate the targeting ligands to SPIONs surface. To maximize targeting efficiency, various targeting ligands,

* Corresponding author at: School of Materials Science and Engineering, Key Laboratory of Advanced Technologies of Materials, Ministry of Education, Southwest Jiaotong University, Chengdu 610031, PR China. Tel.: +86 2887634023; fax: +86 2887634649.
E-mail addresses: shaobingzhou@swjtu.cn, shaobingzhou@hotmail.com (S. Zhou).

0378-5173/$ – see front matter © 2012 Elsevier B.V. All rights reserved.
doi:10.1016/j.ijpharm.2012.03.001

such as small peptides and aptamers, can be chosen for the cell-specific targeting strategies. Besides, a surface marker (antigen or receptor) should be overexpressed on the targeted cells relative to the normal cells (Lee et al., 2009; Peer et al., 2007). One of the promising targeting ligands in cancer treatments is folic acid (FA), since folate receptors exhibit limited expression on healthy cells, but over-expressed in a range of tumor including breast, ovarian, liver and kidney cancers (Peer et al., 2007; Zhang et al., 2010). The SPIONs binding of FA ligands can be efficiently taken up by specific cell *via* receptor-mediated cellular uptake. This folate receptor targeted delivery is very effective *in vitro*, however, it failed to increase drug concentrations in tumors *in vivo* due to the heterogeneity of tumors and the accessibility of tumor cell surface targets to the drug delivery system (Pradhan et al., 2010; Lowery et al., 2011). Therefore, Park (2010) thinks that the true targeted delivery of drug delivery systems *in vivo* has not been achieved, and only a small fraction of the administered particles reach the target site.

Design of the novel nanofabricated systems is greatly expected for targeted drug delivery. Herein, the fabrication of multifunctional magnetic nanomicelles for targeted drug delivery system was investigated. The formulation of the drug loaded magnetic nanomicelles include the FDA-approved biocompatible copolymers Pluronic F127 and poly (DL-lactic acid) (PLA–F127), which can prolong circulation time of nanocarriers in the body and enhance permeability at the tumor site (Huang et al., 2011), folate moiety, which exhibits strong tumor-actively targeting capability, DOX·HCl as a model anticancer drug, which causes DNA damage *via* intercalate in DNA and interacts with topoisomerase II when accumulate in the cell nucleus (Pradhan et al., 2010).The targeting effects were investigated *in vitro* by the uptakes of tumor cells and normal fibroblast cells of the DOX-loaded nanomicelles in the presence or the absence of a permanent magnetic field. Additionally, the drug-loaded magnetic nanomicelles could be guided to anticipated targeting site by application of a permanent magnet in VX2 tumor-bearing male New Zealand white rabbits, thereby the therapeutic effects of drug were improved obviously.

2. Experimental

2.1. Materials

The F127-PLA polymer ligands modified SPIONs (SPIONs@F127-PLA) were prepared as our previous reports (Huang et al., 2011; Sun et al., 2007). Folic acid (FA) was purchased from Chengdu KeLong Chemical Reagent Company (Sichuan, China) and used as received. Pluronic F127 was purchased from Aldrich (USA) and used as received. Poly(DL-lactic acid) (PLA, Mn 600) was synthesized as our previous report (Zhou et al., 2004). Alamar blue cell viability reagent was purchased from Invitrogen (USA). DOX·HCl was purchased from Zhejiang Hisun Pharmaceutical (China).

The HepG2 (human liver carcinoma cells over-expressing folate receptor) and NIH3T3 (mouse fibroblast limit-expressing folate receptor) cells were purchased from Sichuan University (China). Permanent magnetic field was provided by permanent magnets placed directly underneath the cell culture plate. The magnetic field strength was measured by Gaussmeter (HT 201 Hengtong Magnetoelectricity, Co., Ltd., China). And two different magnetic field strength: the weaker magnetic field strength (M1) = 0.01 T and the higher magnetic field strength (M2) = 0.1 T were obtained *via* adjusting the distance between cell culture plate and permanent magnets.

All animal work was reviewed and approved by the Department of Experimental Animals, Soochow University (Suzhou, China).

2.2. Synthesis of SPIONs@F127-PLA–FA

The SPIONs@F127-PLA–FA was prepared according to the literature (Lin et al., 2009). In brief, 0.2 mmol of FA was dissolved in dried dimethyl sulfoxide (DMSO), and activated by adding both 0.12 mmol N-(3-dimethylaminopropyl)-N′-ethylcarbodiimide hydrochloride (EDC) and 4-dimethy-laminopyridine (DMAP). The mixture was stirred overnight. Next, 0.1 mmol 3-(triethoxysily) propyl isocyanate (TPI) was added to the resultant solution overnight. Then, 20 mg SPIONs@F127-PLA and 10 μL Et_3N were added into the resultant solution overnight under nitrogen. Finally, all products were collected with a magnet and washed several times with ethanol and water. Then, freeze-dried and stored at −4 °C for further use.

2.3. Characterization

FT-IR (Nicolet 5700) and UV–visible spectrophotometry (UV-2550, Shimadzu, Japan) was performed to analyze the structure of all samples. The morphology was observed by TEM (HITACHI H-700H) at an accelerating voltage of 175 kV. Particle size and its distribution were determined by Particle Size Analyzer (ZETASIZER, MALVERN Nano-ZS90). The maximum loading amount of DOX·HCl in the magnetic nanomicelles was determined by Fluoromax spectrometer (F-7000, HITACH, Japan).

2.4. Drug loading and in vitro release

The maximum loading amount of DOX·HCl was determined by serial addition of the magnetic nanomicelles to DOX·HCl solution. The fluorescence of DOX·HCl was quenched when the compounds were absorbed into the micelles (Yu et al., 2008; Guo et al., 2009). The *in vitro* drug release from the magnetic nanomicelles was studied by using a dialysis membrane (MWCO 14,000) in an acetate buffered solution (ABS, pH 5.1) and a phosphate buffered solution (PBS, pH 7.4). The DOX·HCl-loaded magnetic nanomicelles were transferred to a dialysis membrane and immersed into 20 mL PBS and ABS separately at 37 °C companying with a gentle shake. At appropriate intervals, 1.0 mL release medium was collected and 1.0 mL fresh buffer solution was added back. The amount of DOX·HCl release was determined by UV–visible spectrophotometer.

2.5. In vitro cytotoxicity

NIH3T3 cells were cultured in DMEM medium supplemented with 10% fetal bovine serum (FBS) at 37 °C in a 5% CO_2 incubator. And the HepG2 cells were cultured in RPMI 1640 medium supplemented with 10% FBS at 37 °C in a 5% CO_2 incubator. For the cytotoxicity test, HepG2 cells were seeded in 24-well tissue culture plates at a density of 1×10^4 cells per well in medium. After 24 h, the culture mediums were replaced with medium containing the various concentrations of the samples. The Alamar blue assay was performed after a culture period of 1, 2 and 3 days. Each well was added with 280 μL Medium 199 (Ml99), 10 μL FBS and 10 μL Alamar blue agent for 4 h. Then the absorbance of the medium was read at 570 nm with ELISA microplate reader (mQ×200, BIO-TEK, USA) against a medium-blank with Alamar blue agent. The difference of the absorbances between $E_{570\,nm,\,cells}$ and $E_{570\,nm,\,blank}$ was linear with the number and activity of the cells (Brien et al., 2000; Martina et al., 2005).

2.6. Antiproliferative activity analysis

For the antiproliferative activity test, HepG2 cells were seeded at 5000 cells per well in 96-well plates and were allowed to attach

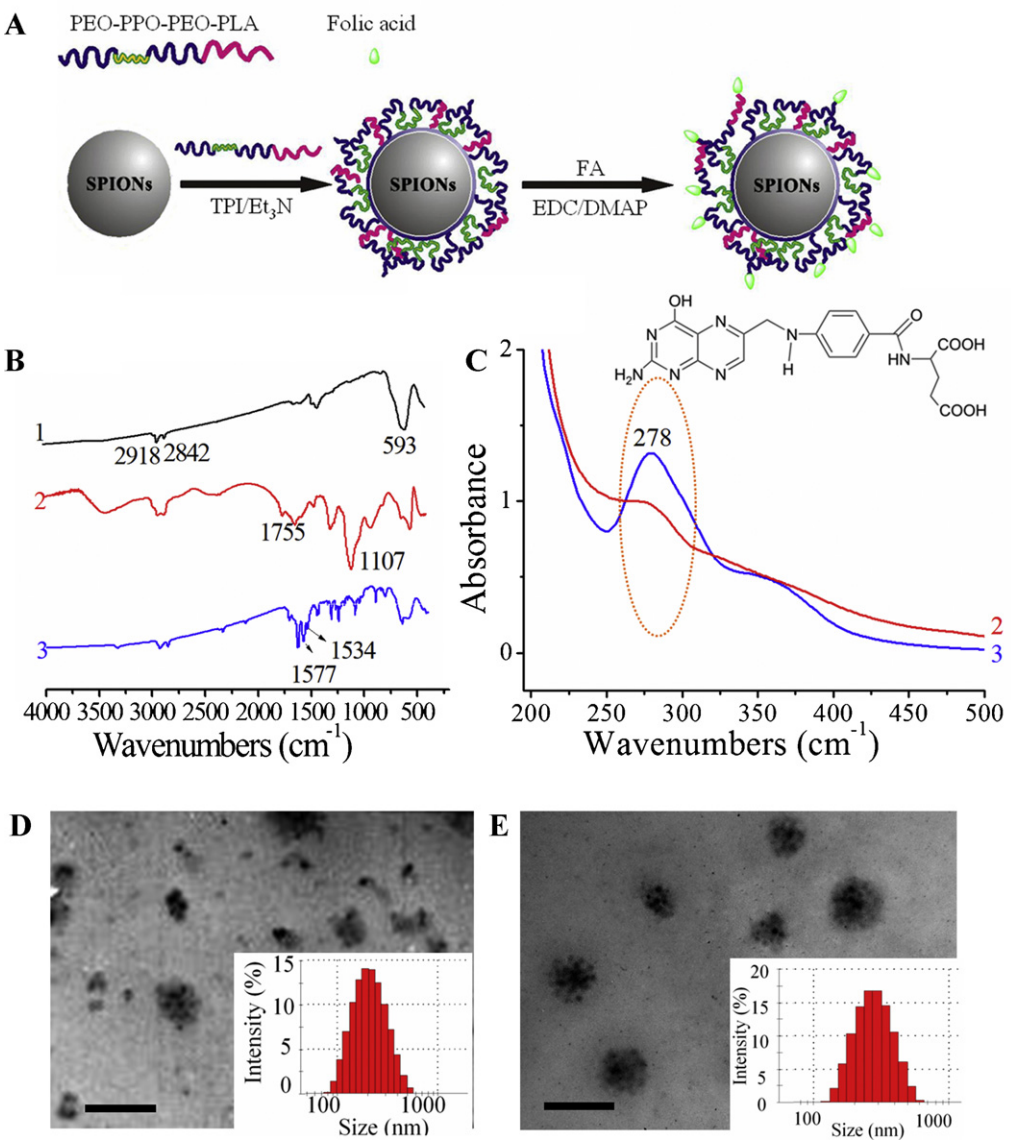

Fig. 1. Schematic route of synthesis of SPIONs@F127-PLA–FA (A); FT-IR spectra (B); UV–vis spectra, of SPIONs (1), SPIONs@F127-PLA (2) and SPIONs@F127-PLA–FA (3) (C); TEM images of SPIONs@F127-PLA (D) and SPIONs@F127-PLA–FA (E) (scale bar, 50 nm, the inset is size distribution of the nanomicelles).

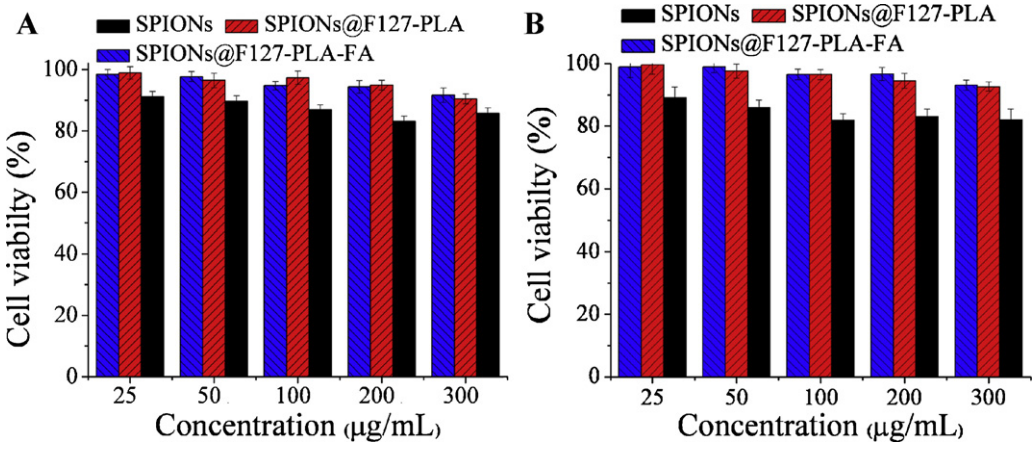

Fig. 2. The Alamar blue assay of HepG2 cells growth on the different concentration of the magnetic nanomicelles without M2 (A) and with M2 (B).

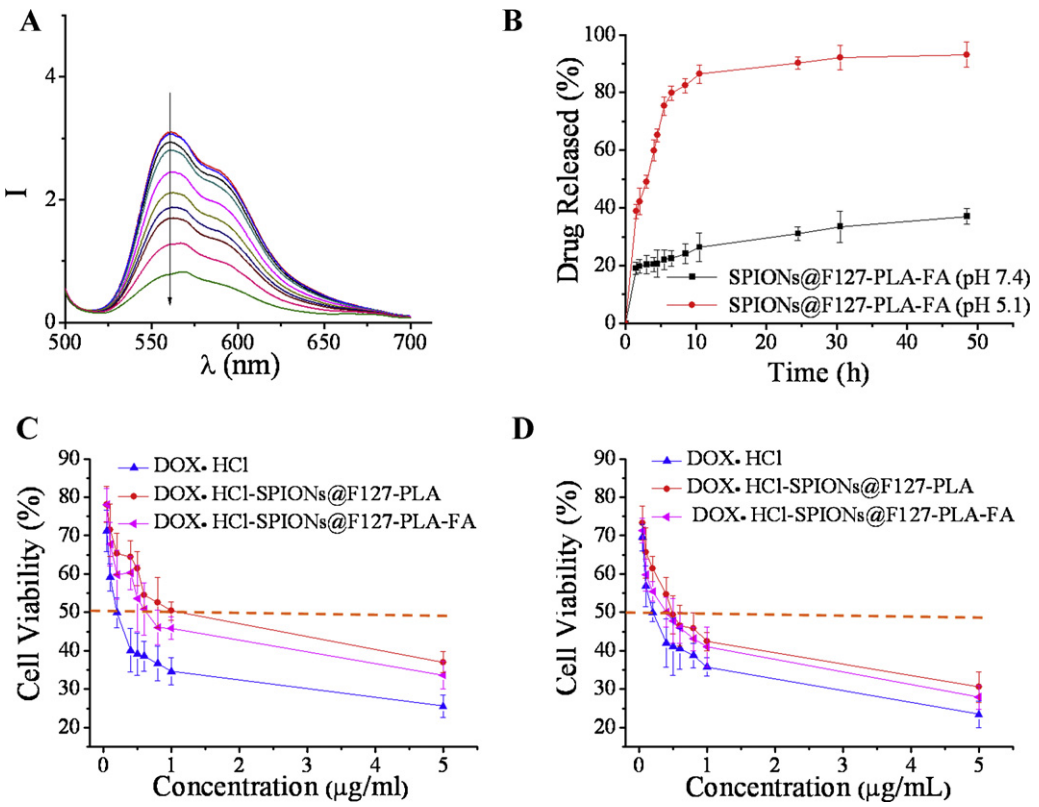

Fig. 3. Fluorescence spectra of DOX·HCl solution (0.1 mg in 3 mL of PBS solution) with increasing mass weight of SPIONs@F127-PLA–FA from bottom to top: 5.532, 3.688, 2.459, 1.093, 0.728, 0.486, 0.324, 0.216, 0.144, 0.096 mg (A); the release behavior of DOX·HCl over a 50 h period at pH 7.4 and 5.1 (B); antiproliferative effect of drug in solution and loaded in magnetic nanomicelles without M2 (C) and with M2 (D) in HepG2 cells.

for 1 day. The cells were treated either with the drug solution or the drug-loaded magnetic nanomicelles at different doses with or without permanent magnetic field. The antiproliferative activity of drug loaded magnetic nanomicelles was determined by Alamar blue assay.

2.7. In vitro cellular uptake of the magnetic nanomicelles

For fluorescent microscope study, HepG2 cells were seeded in 24-well tissue culture plates at a density of 1×10^4 cells per well in the medium with or without permanent magnetic field. The drug-loaded magnetic nanomicelles dispersed in the cell culture medium at drug concentrations of 2 μg/mL were added into the wells. After incubation with samples for 6 h, the cells were fixed with 3% formaldehyde and washed with PBS. The internalization of all samples at different condition was visualized by fluorescence microscope (Olympus IX51, Japan) and the relative fluorescence intensity was analyzed using Image-Pro Plus 6.0 software. The samples were then examined with laser confocal scanning microscopy (CLSM) (Leica TCS SP2 Germany) and flow cytometry (Epics Elite EST, USA).

Prussian blue staining was also performed to reveal the presence of iron cations with or without the referred magnetic field. After incubation with the samples at the concentrations of 100 μg/mL for 6 h, the cells were fixed with 3% formaldehyde and washed with PBS, followed by the incubation with 2% potassium ferrocyanide in 6% hydrochloric acid for 30 min. Then, the samples were examined with an optical microscope.

2.8. In vivo tumor accumulation and anti-tumor effect in tumor-bearing rabbits

Animals, New Zealand white rabbits (2.5–3.0 kg), were acclimatized at a temperature of 25 °C and a relative humidity of 40–70%, and given access to food and water *ad libitum*. A tumor model was established in New Zealand white rabbits bearing VX2 tumor over-expressing folate receptors according to literature (Maeng et al., 2010). VX2 rabbit tumor nodule was cut into small pieces (about 1 mm × 1 mm × 1 mm) and then implanted into the both leg of rabbits. When the tumor nodules had reached a volume of 18 mm × 13 mm × 10 mm (approximately 2 weeks post-implantation), the *in vivo* experiment were performed.

24 rabbits were randomly divided into three groups, each group had eight rabbits, and they are described as follow: (1) control groups: rabbits were treated without any injection; (2) SPIONs@F127-PLA–FA without M2: rabbits were injected *via* the ear vein with SPIONs@F127-PLA–FA (5 mg/kg per rabbits); and (3) SPIONs@F127-PLA–FA with M2; a permanent magnet (M2 = 0.1 T) was placed at the tumor site of the rabbits leg. And then the rabbits were injected *via* the ear vein with SPIONs@F127-PLA–FA (5 mg/kg). For Prussian blue staining *in vivo*, after injection SPIONs@F127-PLA–FA for 12 h, both tumor tissue of the control groups, SPIONs@F127-PLA–FA without M2 groups and the PIONs@F127-PLA–FA with M2 groups were excised and stored in 10% formalin. Paraffin-embedded histological slices were stained with Prussian blue staining (Kainthan et al., 2006). To estimate the effect of drug loaded magnetic nanomicelles on suppressing the growth of tumor under the condition of a permanent magnet, the hematoxylin–eosin (HE) staining and the color Doppler ultrasound imaging (Mindray M5 color Doppler ultrasonography) were carried out to localize and monitor the tumor issue. The rabbits

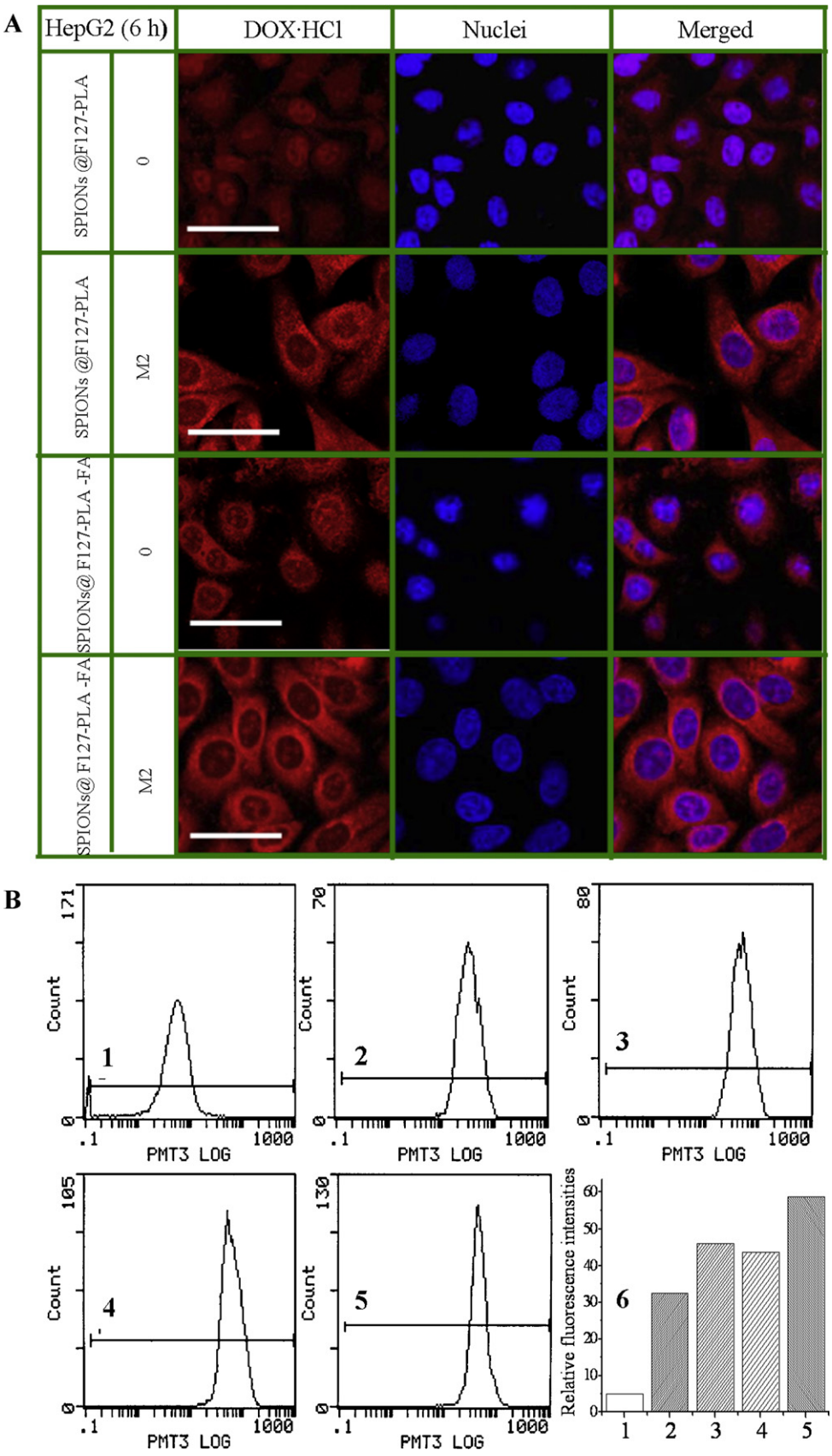

Fig. 4. Confocal microscopy analysis (A) of HepG2 cells after 6 h incubation with magnetic nanomicelles without (0) or with M2 (scale bar, 50 μm). The nuclei were stained with DAPI. Flow cytometry (B) of the uptake of magnetic nanomicelles by HepG2 cells for 6 h: (1) control group, (2) SPIONs@F127-PLA without M2, (3) SPIONs@F127-PLA with M2, (4) SPIONs@F127-PLA–FA without M2, (5) SPIONs@F127-PLA–FA with M2 and (6) the corresponding relative fluorescence intensities.

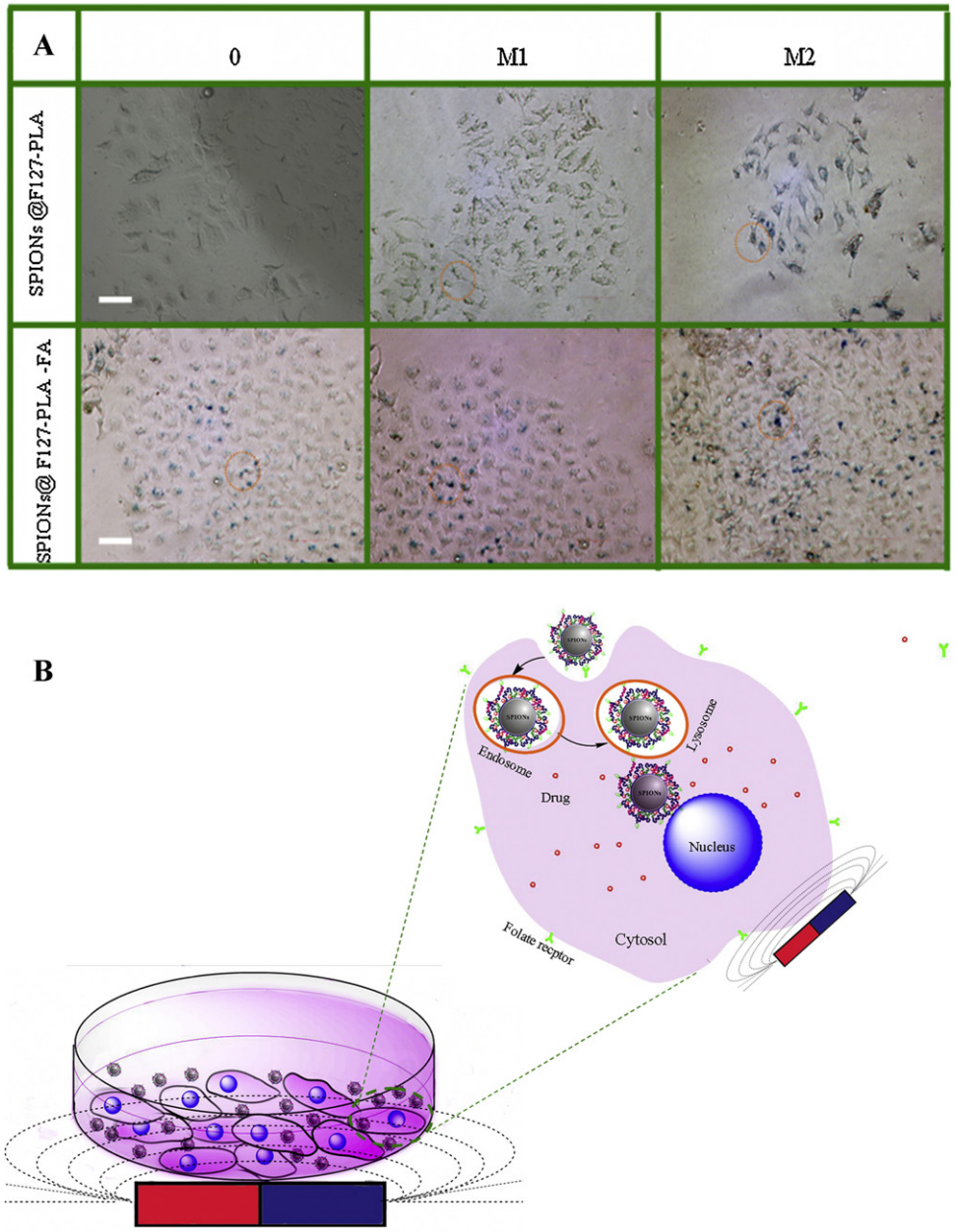

Fig. 5. Prussian blue staining (A) of HepG2 cells after 6 h incubation with magnetic nanomicelles without (0) or with permanent magnetic field at different strength (M1 and M2) (scale bar, 50 μm), and the schematic illustration (B) of drug delivery of SPIONs@F127-PLA–FA under the magnetic field.

were given two intravenous doses administered every week. On each treatment day, permanent magnetic field was applied for 2 h after injection with SPIONs@F127-PLA–FA. After administration for 2 weeks, the tumor tissue was excised for HE staining and examined by color Doppler ultrasound imaging.

3. Results and discussion

3.1. Characterization of the magnetic nanomicelles

The fabrication of SPIONs@F127-PLA–FA was illustrated in Fig. 1A. Firstly, SPIONs coated with OA were obtained by the classical chemical coprecipitation method. Later, SPIONs@F127-PLA was synthesized *via* ligand exchange with F127-PLA copolymer, after that FA was conjugated to the SPIONs@F127-PLA by condensation reaction between terminal hydroxyl groups of F127-PLA and carboxyl groups of FA. To demonstrate the successful synthesis of SPIONs@F127-PLA–FA, the FT-IR was carried out, and Fig. 1B represented the FT-IR spectrum of SPIONs, SPIONs@F127-PLA and SPIONs@F127-PLA–FA. In Fig. 1B1, the peaks at 2918 cm^{-1} and 2847 cm^{-1} were ascribed to the $-CH_3$ and $-CH_2-$ of OA, and the peak at about 593 cm^{-1} was due to the vibration of Fe–O. In Fig. 1B2, the peaks in the range of 1250–1000 cm^{-1} were attributed to C–O–C stretching and $-CH_2-$ rocking vibrations in the PEO–PPO–PEO chains of F127 (Jain et al., 2009), and the peak at 1755 cm^{-1} due to the ester band in SPIONs@F127-PLA. In Fig. 1B3, the peaks in the range of 1534–1694 cm^{-1} belonged to aromatic ring stretch in the pyridine and benzene ring of FA (Setua et al., 2010). To further verify the successful synthesis of SPIONs@F127-PLA–FA, UV–visible spectrum was also performed at each step of the synthesis. In Fig. 1C, the peaks at wavelength 278 nm were considered as characteristics of FA due to the aromatic ring in SPIONs@F127-PLA–FA (Bagalkot

et al., 2006). TEM and particle size analyzer were used to observe the morphology and particle distribution of SPIONs@F127-PLA and SPIONs@F127-PLA–FA (Fig. 1D and E). Both samples aggregated to form clusters which composed of small iron oxide nanoparticles with a size about 10 nm, furthermore, the size distribution showed that the *z*-average diameter values of the SPIONs@F127-PLA and SPIONs@F127-PLA–FA were 236 nm and 265 nm, respectively.

3.2. Cytotoxicity analysis

To examine the cytotoxicity of the magnetic nanomicelles stimulated with or without permanent magnetic field, HepG2 cells were incubated with all samples in the concentrations ranging from 25 to 300 μg/mL for 1 day. As can be seen in Fig. 2A and B, both SPIONs@F127-PLA and SPIONs@F127-PLA–FA showed no toxicity at all tested concentrations in the presence or absence of permanent magnetic field (M2), by contrast, the cell viability decreased when incubation with unmodified SPIONs at the concentration of 300 μg/mL. The results indicated that the toxicity of SPIONs would be reduced after modification with the biocompatible polymer, and there was little influence on cell viability in the presence of a magnetic field.

3.3. Drug release behaviors

The maximum loading amount of DOX·HCl in the nanomicelles can be obtained by testing the intensity of auto-fluorescence of the drug. When a fixed concentration of DOX·HCl was incubated with increasing amounts of SPIONs@F127-PLA–FA, the sequential decreases in the native fluorescence spectrum of DOX·HCl were observed. In Fig. 3A, the maximal quenching of DOX·HCl fluorescence was achieved with approximate 0.1 mg DOX·HCl to 5.532 mg SPIONs@F127-PLA–FA, indicating that the optimal loading amount of DOX·HCl to SPIONs@F127-PLA–FA were about 1.8%.

Fig. 3B shows the *in vitro* release behaviors of DOX·HCl at different pH values over 50 h. The release profiles presented that SPIONs@F127-PLA–FA had exhibited a sustained release behavior at pH 7.4, the amount of DOX·HCl released from SPIONs@F127-PLA–FA reached 37.08%, on the other hand, the release behavior of DOX·HCl proceeded much faster at pH 5.1 than pH 7.4, which was in agreement with previous reports (Bagalkot et al., 2006; Chen et al., 2009; Yang et al., 2008). Approximately 93.1% of the drug was released from SPIONs@F127-PLA–FA at pH 5.1. This might be due to the final concentration of DOX·HCl in the environmental solution determined by its solubility which was pH-dependent (Chen et al., 2009).

3.4. Antiproliferative effect of the DOX·HCl-loaded magnetic nanomicelles

The antiproliferative effect of the DOX·HCl-loaded magnetic nanomicelles were determined by Alamar blue assay. Fig. 3C and D exhibited that both of the DOX·HCl-loaded magnetic nanomicelles and free DOX·HCl had a dose-dependent effect on HepG2 cell antiproliferative with or without the magnetic field (M2). Without M2 the IC_{50} values of free DOX·HCl, DOX·HCl-loaded SPIONs@F127-PLA and DOX·HCl-loaded SPIONs@F127-PLA–FA were 0.2 mg/mL, 1 mg/mL and 0.6 mg/mL, respectively. By contrast, with M2 the IC_{50} values of free DOX·HCl, DOX·HCl-loaded SPIONs@F127-PLA and DOX·HCl-loaded SPIONs@F127-PLA–FA were 0.2 mg/mL, 0.5 mg/mL and 0.4 mg/mL, separately. The cell viability of the cancer cells with free DOX·HCl was lower than that with DOX·HCl-loaded magnetic nanomicelles at the same concentration with or without M2. The reason may be that the magnetic nanomicelles could decrease the toxicity of the drug applied due to the controlled and sustained efficacy of the drug release, consequently, they also would increase the maximum tolerance dose (MTD). When exposing the drug with high concentration instantly in blood, it was presumed to be toxic not only for the cancer cells but also for the normal cells (Liu et al., 2010). Additionally, the cell viability of DOX·HCl-SPIONs@F127-PLA was higher than DOX·HCl-SPIONs@F127-PLA–FA at the same condition. The result suggested that SPIONs@F127-PLA–FA bearing the FA could be targeted to the HepG2 cells which over-express folate receptors. Therefore the concentrations of drug inside tumor cells would increase through receptor-mediated targeting (Cheng et al., 2011). On the other hand, in the presence of M2, the cell viability of DOX·HCl-SPIONs@F127-PLA and DOX·HCl-SPIONs@F127-PLA–FA were decreased obviously (according to IC_{50} values), and the difference of the cell viabilities between all samples were reduced. These results indicated that the treatment efficacy of the drug would be enhanced by application of M2, when subjected to the magnetic field, the nanomicelles were attracted to be oriented and targeted to the cells directly.

3.5. The targeted drug delivery of the DOX·HCl-loaded magnetic nanomicelles

To examine the intracellular delivery of the DOX·HCl-loaded magnetic nanomicelles, all samples were incubated with HepG2 cells and NIH3T3 fibroblast cells with or without different magnetic field strength (M1 and M2) at different incubation period. In Supporting information, Fig. SA–D showed the fluorescence images and the relative fluorescence intensities at different conditions. The intrinsic fluorescence (red) of the DOX·HCl-loaded magnetic nanomicelles were observed in some areas of NIH3T3 cells after incubation for 6 h, both samples showed the similar fluorescence intensities in the absence of magnetic field, meanwhile, the fluorescence signal became more stronger while the magnetic field strength increased gradually (Fig. SA). It was worthily noticed that there were no distinct difference between DOX·HCl-SPIONs@F127-PLA and DOX·HCl-SPIONs@F127-PLA–FA at the same conditions, and the relative fluorescence intensities also confirmed these results. Fig. SB–D showed the fluorescence images and the relative fluorescence intensities of HepG2 cells incubated with the DOX·HCl-loaded magnetic nanomicelles at different incubation period. Comparing those data, we could found that the fluorescence signal was enhanced with increasing incubation time, and the fluorescence signal of DOX·HCl-SPIONs@F127-PLA was weaker than DOX·HCl-SPIONs@F127-PLA–FA at the same conditions, moreover the fluorescence signal dramatically increased with the magnetic field strength being increased.

To further verify the influences of FA ligands and permanent magnetic field (M2), the cellular uptake image of magnetic nanomicelles into HepG2 cells for 6 h incubation was directly visualized by CLSM (Fig. 4A), and the corresponding quantitative cellular uptake analysis was determined by flow cytometry (Fig. 4B). As can be seen, the red fluorescent color of all samples was found surrounding the nucleus obviously, which demonstrated that the magnetic nanomicelles could carry and release drug into the cells following the cancer cells internalization. And the presence of FA ligands and the magnetic field enhanced the internalization of the magnetic nanomicelles. In particular, it was noticed that the cellular uptake of the magnetic nanomicelles might depend more strongly on the magnetic field rather than FA moiety, which was also demonstrated by the flow cytometry analysis.

Fig. 4B exhibited that the relative fluorescence intensities of control group, SPIONs@F127-PLA with or without M2, and SPIONs@F127-PLA–FA with or without M2 were 5, 46, 32.5, 58.7 and 43.6, respectively. The result further confirmed the following phenomena collectively: the cellular uptake efficiency of the SPIONs@F127-PLA-FA was enhanced significantly compared with

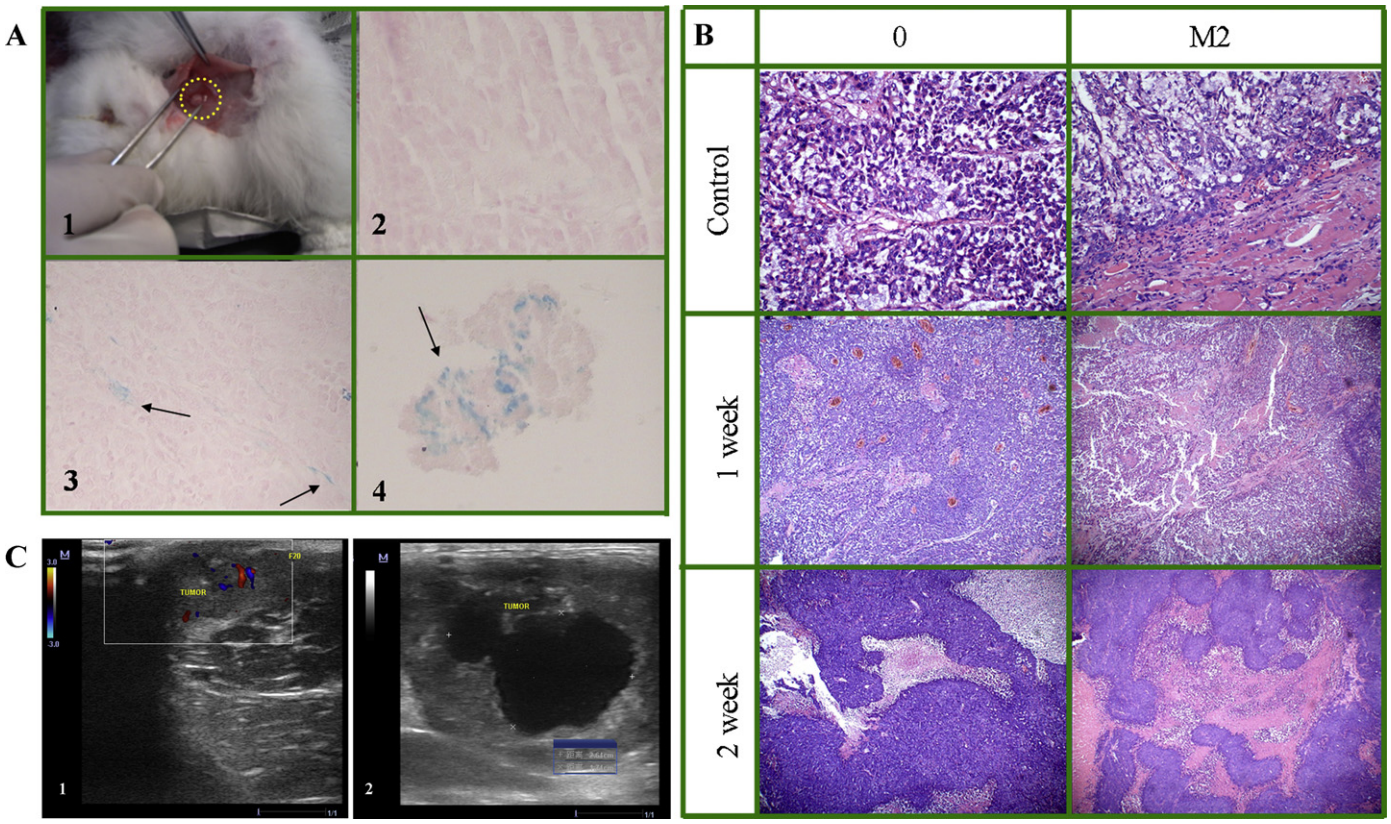

Fig. 6. Prussian blue staining (A) (magnification 400×): (1) the picture of rabbits bearing tumor (2) control group, (3) SPIONs@F127-PLA–FA without M2, (4) SPIONs@F127-PLA–FA with M2, HE staining (B) (magnification 200×) and the color Doppler ultrasound images (C) of the tumor tissues of the magnetic nanomicelles: (1) control group and (2) SPIONs@F127-PLA–FA with M2.

SPIONs@F127-PLA under the same condition when incubation with HepG2 cells bearing over-expressed folate receptors, on the other hand, when incubation with NIH3T3 cells without over-expressed folate receptors, there was no remarkable difference of cellular uptake efficiency between SPIONs@F127-PLA–FA and SPIONs@F127-PLA. That may indicate that folate receptor targeting would enhance the cellular uptake efficiency of the nanomicelles *via* receptor-mediated endocytosis, thereby therapeutic efficacy of anticancer drug was increased due to the shifting of drug distribution from the extracellular to the intracellular compartment (Pradhan et al., 2010; Liu et al., 2010). Meanwhile, the enhanced intracellular drug delivery under the action of the permanent magnetic field could be due to the following reasons: (1) the magnetic nanomicelles were orientated and sedimented at the cell surface; (2) the magnetic nanomicelles would be through the cell membrane, and the endocytosis or other process were facilitated (Wu et al., 2010; Pradhan et al., 2010). In addition, this result was also verified by following animal experiment.

Prussian blue staining was also performed to detect iron oxide which stains blue. In Fig. 5A, all the magnetic nanomicelles appeared blue due to the formation of Prussian blue precipitates inside the cells, which indicated that all samples were internalized into the cells. Simultaneously, the blue colour inside HepG2 cells was clearer in presence of FA and the permanent magnetic field (M1 and M2), suggesting that the larger amount of iron oxides were uptaken. Fig. 5B illustrated the process of the intracellular delivery of DOX·HCl-SPIONs@F127-PLA–FA nanomicelles. Firstly, the magnetic micelles was guided and maintained to the cell surface by application of a magnetic field, and then bound to the cell surface *via* the synergistic action of receptor-mediated endocytosis and magnetic force, and then internalization of the nanoparticles by the specific endocytosis pathway (Zhang et al., 2009; Ganta et al., 2008). After internalized into the cytoplasm, they were engulfed by endosomes which formed *via* membrane invagination (Lee et al., 2010). Finally, it accumulated in acidic lysosomes (pH 4–5) and the release rate of the pH-dependent drug was accelerated (Zhou et al., 2009).

3.6. Targeted delivery and therapeutic efficacy of drug loaded magnetic nanomicelles in vivo

Preliminary *in vivo* tumor model study was employed to check whether the magnetic micelles possess targeting property in the presence of an external magnetic filed. To validate the targeting specificity of the magnetic nanomicelles *in vivo*, Prussian blue staining of the tumor tissues was performed. As shown in Fig. 6A1, the tumor was implanted subcutaneously in the foot of rabbit. In Fig. 6A2, the tumor issues without administration were stained by Prussian blue staining, and the blue color was not found in this area. In Fig. 6A3 and A4 those tumor tissues were eviscerated after injected with SPIONs@F127-PLA–FA 12 h with or without a magnetic field. As shown in Fig. 6A3 without the magnetic field, Prussian blue staining appeared only in few regions, which indicated that small amount of SPIONs@F127-PLA–FA diffused in blood vessel in the absence of permanent magnetic field. In contrast, an enrichment of the particles in tumor was found with Prussian blue staining in Fig. 6A4 with the magnetic field (M2). It demonstrated large amount of nanomicelles accumulated in the areas of tumor due to the presence of M2. It also indicated that the external magnetic field can guide the magnetic nanomicelles to targeted site.

HE staining of tumor tissues from rabbits was shown in Fig. 6B. In the control group, the tumor cells proliferated heavily, arrayed regularly, and invaded the surrounding musculature. By contrast, the tumor tissues revealed that a small area of tumor necrosis

region appeared in SPIONs@F127-PLA–FA treated in the presence of M2 after 1 week administration, and the nanomicelles induced extensive tumor necrosis after 2 weeks administration. However, without the magnetic field, there were only small area of tumor necrosis region appeared in the period of 1 and 2 weeks.

To further examine the therapeutic efficacy of drug loaded SPIONs@F127-PLA–FA in the presence of M2, the rabbits bearing VX-2 tumor were treated with the DOX-loaded micelles (5 mg/kg SPIONs@F127-PLA–FA and 0.09 mg DOX·HCl). The color Doppler ultrasound imaging was carried out to localize and monitor the tumor. As shown in Fig. 6C1 and C2, before treating with drug, the dimension of the tumor issues was 18 mm × 13 mm × 10 mm (Fig. 6C1), after treating with drug for 2 weeks, the dimension of the tumor issues increased to 36 mm × 23 mm × 15 mm (Fig. 6C2), and the morphology of the tumor issues became more irregular. It was noteworthy that there was a cavum filled with necrotic liquid in the center of the tumor issues (Fig. 6C2), which indicated that the tumor issues began to necrosis. The result also suggested that more drug-loaded magnetic nanoparticles should be concentrated on the tumor site in the presence of the external field. If the nanoparticles were not guided by the field, they could be delivered passively to tumor site. Thus the concentration of drug must be low, which leads to poor therapy effect to tumor.

The above primary pictures demonstrated qualitatively that the magnetic nanomicelles can be guided to targeted site by the aid of external magnetic field, and correspondingly the therapeutic efficacy of anti-tumor drug can be improved. These qualitative results were carried out with simply statistical analysis, which suggested that the dual targeting micelles can lead to better therapeutic results. Of course, based on them, in the future it will be very necessary and interesting to study *in vivo* antitumor function from the change of tumor volume, body weight loss, survival rate and the immunostaining of tumor sections systematically.

4. Conclusion

In this work, the magnetic nanomicelles were successfully fabricated for targeted drug delivery by incorporation of active targeted ligands and magnetic-guided superparamagnetic nanoparticles. The cell viabilities studies displayed that the magnetic micelles were safe carriers as drug vehicles. The results from fluorescent microscopy, CLSM and flow cytometry indicated that the targeting efficacy of the folic acid modified magnetic nanomicelles was enhanced for the HepG2 cells of over expression of folate receptors and unimproved significantly for the normal fibroblasts. In particular, the efficiency and veracity of drug delivery were improved evidently *in vitro* and *in vivo* by application of a permanent magnetic field. In a word, the efficiency of the intracellular uptake of the nanomicelles could be enhanced by the aids an external magnetic field, and thus the therapeutic effect of drug could be improved. Therefore, the magnetic nanomicelles as nanocarriers possessed great potential for dual targeted drug delivery in cancer therapy.

Acknowledgements

This work was partially supported by National Natural Science Foundation of China (Nos. 30970723 and 51173150) and National Basic Research Program of China (973 Program, 2012CB933602).

Appendix A. Supplementary data

Supplementary data associated with this article can be found, in the online version, at doi:10.1016/j.ijpharm.2012.03.001.

References

Allen, T.M., Cullis, P.R., 2004. Drug delivery systems: entering the mainstream. Science 303, 1818–1822.
Bagalkot, V., Farokhzad, O.C., Langer, R., Jon, S.Y., 2006. An aptamer–doxorubicin physical conjugate as a novel targeted drug-delivery platform. Angew. Chem. Int. Ed. 45, 8149–8152.
Brien, J.O., Wilson, I., Orton, T., Pognan, F., 2000. Investigation of the Alamar Blue (resazurin) fluorescent dye for the assessment of mammalian cell cytotoxicity. Eur. J. Biochem. 267, 5421–5426.
Chen, L.B., Zhang, F., Wang, C.C., 2009. Rational synthesis of magnetic thermosensitive microcontainers as targeting drug carriers. Small 5, 621–628.
Cheng, Z., Thorek, D., Tsourkas, A., 2011. Coupling of luminescent terbium complexes to Fe_3O_4 nanoparticles for imaging applications. Angew. Chem. Int. Ed. 50, 3063–3066.
Fan, C., Gao, W., Chen, Z., Fan, H., Li, M., Deng, F., Chen, Z., 2011. Tumor selectivity of stealth multi-functionalized superparamagnetic. Int. J. Pharm. 404, 180–190.
Ganta, S., Devalapally, H., Shahiwala, A., Amiji, M., 2008. A review of stimuli-responsive nanocarriers for drug and gene delivery. J. Control. Release 126, 187–204.
Gautier, J., Munnier, E., Paillard, A., Hervé, K., Douziech-Eyrolles, L., Soucé, M., Dubois, P., Chourp, I., 2011. A pharmaceutical study of doxorubicin-loaded PEGylated nanoparticles for magnetic drug targeting. Int. J. Pharm. 423, 16–25.
Guo, S.J., Li, D., Zhang, L.X., Li, J., Wang, E.K., 2009. Monodisperse mesoporous superparamagnetic single-crystal magnetite nanoparticles for drug delivery. Biomaterials 30, 1881–1889.
Huang, C., Zhou, Y.B., Jin, Y., Zhou, X., Tang, Z.M., Guo, X., Zhou, S.B., 2011. Preparation and characterization of temperature-responsive and magnetic nanomicelles. J. Mater. Chem. 21, 5660–5670.
Hou, C.H., Hou, S.M., Hsueh, Y.S., Lin, J., Wu, H.C., Lin, F.H., 2009. The in vivo performance of biomagnetic hydroxyapatite nanoparticles in cancer hyperthermia therapy. Biomaterials 30, 3956–3960.
Jain, T.K., Foy, S.P., Erokwu, B., Dimitrijevic, S., Flask, C.A., Labhasetwar, V., 2009. Magnetic resonance imaging of multifunctional pluronic stabilized iron-oxide nanoparticles in tumor-bearing mice. Biomaterials 30, 6748–6756.
Kainthan, R.K., Gnanamani, M., Ganguli, M., Ghosh, T., Brooks, D.E., Maiti, S., Kizhakkedathu, J.K., 2006. Blood compatibility of novel water soluble hyperbranched polyglycerol-based multivalent cationic polymers and their interaction with DNA. Biomaterials 27, 5377–5390.
Ke, J.H., Lin, J.J., Carey, J.R., Chen, J.S., Chen, C.Y., Wang, L.F., 2010. A specific tumor-targeting magnetofluorescent nanoprobe for dual-modality molecular imaging. Biomaterials 31, 1707–1715.
Kim, D.H., Rozhkova, E.A., Ulasov, I.V., Bader, S.D., Rajh, T., Lesniak, M.S., Novosad, V., 2010. Biofunctionalized magnetic-vortex microdiscs for targeted cancer-cell destruction. Nat. Mater. 9, 165–171.
Lattuada, M., Hatton, T.A., 2007. Functionalization of monodisperse magnetic nanoparticles. Langmuir 23, 2158–2168.
Lee, H., Yu, M.K., Park, S., Moon, S., Min, J.J., Jeong, Y.Y., Kang, H.W., Jon, S.Y., 2007. Thermally cross-linked superparamagnetic iron oxide nanoparticles: synthesis and application as a dual imaging probe for cancer in vivo. J. Am. Chem. Soc. 129, 12739–12745.
Lee, P.W., Hsu, S.H., Wang, J.J., Tsai, J.S., Lin, K.J., Wey, S.P., Chen, F.R., Lai, C.H., Yen, T.C., Sung, H.W., 2010. The characteristics, biodistribution, magnetic resonance imaging and biodegradability of superparamagnetic core–shell nanoparticles. Biomaterials 31, 1316–1324.
Lee, J.H., Lee, K., Seung, H.M., Lee, Y.H., Park, T.G., Cheon, J.W., 2009. All-in-one target-cell-specific magnetic nanoparticles for simultaneous molecular imaging and siRNA delivery. Angew. Chem. Int. Ed. 48, 4174–4179.
Lewinski, S., Colvin, V., Drezek, R., 2008. Cytotoxicity of nanoparticles. Small 4, 26–49.
Lin, J.J., Chen, J.S., Huang, S.J., Ko, J.H., Wang, Y.M., Chen, T.L., Wang, L.F., 2009. Folic acid–Pluronic F127 magnetic nanoparticle clusters for combined targeting, diagnosis, and therapy applications. Biomaterials 30, 5114–5124.
Liu, Y.T., Li, K., Pan, J., Liu, B., Feng, S.S., 2010. Folic acid conjugated nanoparticles of mixed lipid monolayer shell and biodegradable polymer core for targeted delivery of docetaxel. Biomaterials 31, 330–338.
Liu, Z., Wang, J., Xie, D.H., Chen, G., 2008. Polyaniline-coated Fe_3O_4 nanoparticle–carbon-nanotube composite and its application in electrochemical biosensing. Small 4, 462–466.
Lowery, A., Onishko, H., Hallahan, D.E., Han, Z.Z., 2011. Tumor-targeted delivery of liposome-encapsulated doxorubicin by use of a peptide that selectively binds to irradiated tumors. J. Control. Release 150, 117–124.
Maeng, J.H., Lee, D.H., Jung, K.H., Bae, Y.H., Park, I.S., Jeong, S., Jeon, Y.S., Shim, C.K., Kim, W., Kim, J.N., Lee, J.L., Lee, Y.M., Kim, J.H., Kim, W.H., Hong, S.S., 2010. Multifunctional doxorubicin loaded superparamagnetic iron oxide nanoparticles for chemotherapy and magnetic resonance imaging in liver cancer. Biomaterials 31, 4995–5006.
Ma, H., Qi, X., Maitani, Y., Nagai, T., 2007. Preparation and characterization of superparamagnetic iron oxide nanoparticles stabilized by alginate. Int. J. Pharm. 333, 177–186.
Martina, M., Subramanyam, G., Weaver, J.C., Hutmacher, D.W., Morse, D.E., Valiyaveettil, S., 2005. Developing macroporous bicontinuous materials as scaffolds for tissue engineering. Biomaterials 26, 5609–5616.
Munniera, E., Cohen-Jonathan, S., Linassiera, C., Douziech-Eyrolles, L., Marchais, H., Soucé, M., Hervé, K., Dubois, P., Chourpa, I., 2008. Novel method of doxorubicin-SPION reversible association for magnetic drug targeting. Int. J. Pharm. 363, 170–176.

Park, K., 2010. Effect of shape and size of polymer particles on cellular internalization. J. Control. Release 147, 313.
Peer, D., Karp, M.J., Hong, S., Farokhzad, O.C., Margalit, R., Langer, R., 2007. Nanocarriers as an emerging platform for cancer therapy. Nat. Nanotechnol. 2, 751–760.
Pradhan, P., Giri, J., Rieken, F., Koch, C., Mykhaylyk, O., Döblinger, M., Banerjee, R., Bahadur, D., Plank, C., 2010. Targeted temperature sensitive magnetic liposomes for thermo-chemotherapy. J. Control. Release 142, 108–121.
Setua, S., Menon, D., Asok, A., Nair, S., Koyakutty, M., 2010. Folate receptor targeted, rare-earth oxide nanocrystals for bi-modal fluorescence and magnetic imaging of cancer cells. Biomaterials 31, 714–729.
Sun, J., Zhou, S.B., Hou, P., Yang, Y., Weng, J., Li, X.H., Li, M.Y.J., 2007. Synthesis and characterization of biocompatible Fe_3O_4 nanoparticles. J. Biomed. Mater. Res. A 80, 333–341.
Wang, B.D., Hai, J., Liu, Z.C., Wang, Q., Yang, Z.Y., Sun, S.H., 2010. Selective detection of iron(III) by rhodamine-modified Fe_3O_4 nanoparticles. Angew. Chem. Int. Ed. 49, 4576–4579.
Wang, L., Yang, Z.M., Gao, J.G., Xu, K.M., Gu, H.W., Zhang, B., Zhang, X.X., Xu, B., 2006. A biocompatible method of decorporation: bisphosphonate modified magnetite nanoparticles to remove uranyl ions from blood. J. Am. Chem. Soc. 128, 13358–13359.
Won, J., Kim, M., Yi, Y.W., Kim, Y.H., Jung, N., Kim, T.K., 2005. A Magnetic nanoprobe technology for detecting molecular interactions in live cells. Science 309, 121–125.
Wu, H.C., Wang, T.W., Bohn, M.C., Lin, F.H., Spector, M., 2010. Novel magnetic hydroxyapatite nanoparticles as non-viral vectors for the glial cell-line derived neurotrophic factor gene. Adv. Funct. Mater. 20, 67–77.
Yang, X.Q., Chen, Y.H., Yuan, R.X., Chen, G.H., Blanco, E., Gao, J.M., Shuai, X.T., 2008. Folate-encoded and Fe_3O_4-loaded polymeric micelles for dual targeting of cancer cells. Polymer 49, 3477–3485.
Yu, M.K., Jeong, Y.Y., Park, J.H., Park, S.J., Kim, J.W., Min, J.J., Kim, K.W., Jon, S.Y., 2008. Drug-loaded superparamagnetic iron oxide nanoparticles for combined cancer imaging and therapy in vivo. Angew. Chem. Int. Ed. 47, 5362–5365.
Zhang, C., Gao, S.J., Jiang, W., Lin, S., Du, F., Li, Z.C., Huang, W.L., 2010. Targeted minicircle DNA delivery using folate-epoly(ethylene glycol)-polyethylenimine as non-viral carrier. Biomaterials 31, 1–12.
Zhang, Y., Yang, M., Park, J.H., Singelyn, J., Ma, H., Sailor, M.J., Ruoslahti, E., Ozkan, M., Ozkan, C., 2009. A surface-charge study on cellular-uptake behavior of F3-peptide-conjugated iron oxide nanoparticles. Small 17, 1990–1996.
Zhou, Z.X., Shen, Y.Q., Tang, J.B., Fan, M.H., Van, K.E., Murdoch, W.J., Radosz, M., 2009. Charge-reversal drug conjugate for targeted cancer cell nuclear drug delivery. Adv. Funct. Mater. 19, 3580–3589.
Zhou, S.B., Deng, X.M., Jia, W.X., Liu, L., 2004. Synthesis and characterization of biodegradable low-molecular-weight aliphatic polyesters and their use in protein delivery system. J. Appl. Polym. Sci. 91, 1848–1856.
Zhu, A., Yuan, L., Liao, T., 2008. Suspension of Fe_3O_4 nanoparticles stabilized by chitosan and o-carboxymethylchitosan. Int. J. Pharm. 350, 361–368.
Zhuo, Y., Yuan, P.X., Yuan, R., Chai, Y.Q., Hong, C.L., 2009. Bienzyme functionalized three-layer composite magnetic nanoparticles for electrochemical immunosensors. Biomaterials 30, 2284–2290.